Research Square

Preprints are preliminary reports that have not undergone peer review.
They should not be considered conclusive, used to inform clinical practice,
or referenced by the media as validated information.

DNA and its rectangular origami nanostructure as substrates for Raman signal enhancement

Rashmi Shrivastava

rshrivastava@rrcat.gov.in

Raja Ramanna Centre for Advanced Technology https://orcid.org/0000-0002-3324-1316

Priya Dangi

Raja Ramanna Centre for Advanced Technology

Aniket Chowdhury

Raja Ramanna Centre for Advanced Technology

Shivangi Verma

Raja Ramanna Centre for Advanced Technology

Chandrachur Mukherjee

Raja Ramanna Centre for Advanced Technology

Kamalika Ghosh

Raja Ramanna Centre for Advanced Technology

Nidhi Maharwal

Raja Ramanna Centre for Advanced Technology

Shovan Majumder

Raja Ramanna Centre for Advanced Technology

Article

Keywords:

Posted Date: May 14th, 2026

DOI: https://doi.org/10.21203/rs.3.rs-9187098/v1

License: This work is licensed under a Creative Commons Attribution 4.0 International License.
Read Full License

Additional Declarations: There is **NO** Competing Interest.

Abstract

Traditional Raman signal enhancement primarily utilizes plasmonic nanostructures to achieve high sensitivity in molecular detection. However, these metallic substrates often encounter significant limitations, including complex fabrication requirements and limited biocompatibility. To address these challenges, we report a novel, metal-free approach using deoxyribonucleic acid (DNA) as a biological macromolecular platform for Raman signal enhancement. By systematically evaluating the Raman response of Rhodamine 6G across three distinct DNA configurations: single-stranded DNA, double-stranded DNA, and rectangular DNA origami nanostructures, we demonstrate that all DNA forms exhibit Raman-enhancing properties. The DNA origami nanostructure provides the most robust signal amplification with enhancement factors approaching 10^2 and detection limits as low as 1×10^{-5} M. These findings suggest that the structural patterning inherent in DNA origami facilitate improved chemical enhancement as compared to ss- or ds-DNA. This approach redefines DNA not merely as a structural template but as a functional Raman-enhancing material for advanced biomedical applications.

Introduction

The fundamental basis of Raman spectroscopy lies in the ability of molecular vibrations to modulate the distribution of the electron cloud under an applied electromagnetic field, thereby altering the molecular polarizability. The resulting inelastic scattering, where the scattered photons differ in energy from the incident photons, probes vibrational or rotational modes that change the molecule's polarizability, thereby generating a structure-dependent spectroscopic fingerprint. Only about 1 in 10^6 -10^8 incident photons undergoes Raman scattering, so the Raman effect is much weaker phenomenon than elastic (Rayleigh) scattering [1]. Since the intensity of the Raman signal is proportional to the polarizability change of the molecule, enhancing the Raman signal requires to induce molecular vibrations that cause the electron cloud around a molecule to distort with ease as the atoms move. Loosely held electrons or extensive π systems usually experience greater changes in polarizability during vibrations, leading to stronger Raman signals[2]. Therefore, Raman signal enhancement can be achieved either through chemical modification or by modulating the molecular environment, which promotes electron cloud delocalization and consequently alters molecular polarizability. The latter being most often explored by choosing or designing systems (environments, excitation wavelengths) so that the natural vibrations lead to significant polarizability variation. Another way may be adding substituents that increase the delocalization of the electron cloud, that may modify the polarizability and its response to vibration[3,4]

Utilizing plasmon-based substrates is one of the common ways to enhance weak Raman signals by leveraging localized surface plasmon resonance[5,6]. This phenomenon amplifies the electromagnetic field in the vicinity of the molecules, thereby increasing the intensity of Raman scattering. Despite their effectiveness in enhancing the signals, plasmon based substrates face several limitations including complex substrate fabrication, limited biocompatibility, and signal reproducibility[7]. In response to these limitations, researchers have explored alternative plasmon free platforms that rely primarily on chemical

enhancement (CE) mechanism. Majorly, CE is based on molecular charge transfer that alters the electron cloud distribution, thereby modulating the polarizability that governs Raman scattering[8]. Examples of these platforms include semiconductor nanostructures, organic crystals like terephthalic acid microcrystals[9], and biocompatible frameworks such as cellulose nanofibers[10], which provide abundant functional groups for analyte binding and charge transfer. More recently, electron rich two-dimensional (2D) materials such as graphene, MoS_2, and h-BN[11] have gained attention as emerging plasmon-free substrates due to their planar geometry and tunable surface chemistry[8].

In this context, biomolecules capable of supporting charge transfer may represent promising alternatives, with deoxyribonucleic acid (DNA) emerging as a particularly interesting candidate. DNA woven by nature as a blueprint of life is more than just a hereditary material or a carrier of genetic information. It is a nanoscale structure with its elegant molecular arrangement of nucleotides forming helices and a remarkable property of self-complementarity that underpins exceptional structural and functional versatility [12]. Basically, DNA is a biopolymer composed of nucleotides where each of its pentose sugar moiety, deoxyribose, is linked to the adjacent nucleotide through a phosphodiester bond and thereby forming the backbone strand. Each sugar is attached to one of the four nitrogenous bases: adenine (A), thymine (T), Cytosine (C), or Guanine(G). In case of double stranded DNA (ds DNA), the two strands run antiparallel and are held together by complementary base pairing (A $=$T and G $\equiv$ C) through hydrogen bonds. All the nitrogenous bases are planar, aromatic structures in which overlapping occurs between adjacent bases leading to π–π stacking interactions and delocalization of π-electrons in the aromatic rings. The over-all DNA double helix structure is stabilized by hydrogen bonds between bases and these base-stacking interactions. DNA, because of its unique self-assembling properties and π-π interactions between its stacked bases, is now at the forefront of emerging technologies like nanofabrication [13], electronics [14], and photonics[15,16]. The π-stacked arrangement of its base pairs facilitates charge migration through mechanisms like tunneling and hopping, highlighting its potential as a molecular-scale conductor or semiconductor[17–19]. Charge transfer via tunneling promote charge delocalization across multiple adjacent bases, and can further extend through electron hopping, enhancing long-range conductivity[20].

Given that DNA supports charge migration, we hypothesize that it may serve as a promising platform for Raman signal enhancement. Moreover, its intrinsic π–π stacking interactions, programmable nanoscale architecture, and capacity for molecular interactions[21–25] further position DNA as a promising candidate for non-metallic Raman-enhancing system. To the best of our knowledge, this aspect remains largely unexplored in the existing literature. In this study, we investigate the potential of different structural forms of DNA—double-stranded DNA (dsDNA), single-stranded DNA (ssDNA), and two-dimensional rectangular DNA origami nanostructures—as metal-free substrates for Raman signal enhancement using Rhodamine 6G (R6G) as a probe molecule. The Raman signal observed on different structural forms of DNA in our study not only establishes DNA as a substrate for Raman enhancement but also suggests how variations in molecular organization, from a floppy ssDNA to highly organized DNA origami influence the signal enhancement.

Results

For Raman signal acquisition a common sample preparation method was employed for all DNA substrates to ensure suitable comparison. For this, various concentrations of R6G were mixed with each of the DNA forms separately in 1xTAE/Mg^{2+} buffer and drop casted onto pre-cleaned glass coverslips (Fig. 1). Upon drying, the Raman signals were measured using an in-house developed micro-Raman setup with 785 nm laser as the Raman excitation source (Supplementary Fig. 1).

Isolation and characterization of dsDNA

A circular plasmid (pcDNA3.1, Addgene)[26] was isolated from *Escherichia coli* (DH5α) host using the standard alkaline lysis method. This plasmid with 7208 bp, served as the model for evaluating Raman signal of R6G on dsDNA substrate. The extracted plasmid was analyzed by agarose gel electrophoresis to confirm its size and conformational forms by running it alongside a 100 -10000 bp DNA ladder. Two distinct characteristic plasmid bands appear, with brightest and farthest corresponding to the supercoiled form, lie near the 8.0 kbp band of the DNA ladder marker while a slower migrating band corresponding to the open circular (nicked) conformation appear far above (Fig. 2a). Further, atomic force microscopy (AFM) was utilized to analyse the morphology of the surface deposited dsDNA. AFM image (Fig. 2b) reveals nanoscale clustered features for dsDNA, consistent with expected morphology of supercoiled plasmid deposited on mica surface[27,28].

Raman signal enhancement of R6G on dsDNA

To investigate the feasibility of Raman signal enhancement on dsDNA, mixtures of varying concentrations of R6G with dsDNA were prepared *a priori*, facilitating the binding of R6G to dsDNA (Fig. 2c). Firstly, the Raman spectra of a mixture of 1×10^{-3} M R6G and ds DNA (50 μg ml^{-1}) were recorded (Fig. 2d) from a dried drop and compared to the respective spectra of only ds DNA and R6G. As evident from Fig. 2d, the Raman spectrum of the dsDNA exhibited a couple of low intensity bands within the spectral range of 600–700 cm^{-1}. It may be noted that the intensity of the characteristic Raman peaks of R6G are much higher and distinct than that of the dsDNA and thus can be clearly identified on the dsDNA substrate. The identified prominent peaks may be attributed to three different modes of vibrations [29] *i.e.* C-C-C ring in- plane bending at 616 cm^{-1}, out of plane bending at 776 cm^{-1}, and ring breathing and aromatic C-C stretching at 1183, 1311, 1361, 1508 cm^{-1}. Rivetingly, an order of magnitude enhancement in the Raman signal of R6G was observed in presence of ds DNA compared to that of the R6G alone. Further, the Raman response of R6G bound to dsDNA was investigated over a concentration range from 5×10^{-4} M to 1×10^{-5} M. As the concentration decreased, the Raman intensity progressively diminished and peaks were undetectable below 1×10^{-4} M for R6G alone; however, distinct Raman peaks remained detectable down to 2.5×10^{-5} M in presence of dsDNA (Fig. 2e). The maximum enhancement factor achieved was 20.

These observations provide the very first evidence that ds DNA can act as a substrate for Raman signal enhancement. These findings motivated us to examine whether the double-helical architecture of dsDNA is required for Raman signal enhancement, or other structural forms, such as ssDNA, can elicit a similar response.

Synthesis and characterization of the ssDNA substrate

For exploring ssDNA as a substrate for Raman signal enhancement, around 200 short oligonucleotides with length ranging from 20 to 35 nucleotides each were synthesized. These were designed and synthesized commercially (see Supplementary Table 1). An equimolar mixture of these was used for Raman spectroscopy of R6G. This cocktail appeared as a diffused band with high mobility rather than a sharp, well-defined band on agarose gel, thereby suggesting the short length and size variability of the ssDNA mixture (Fig. 3a). Nevertheless, the overall migration profile was consistent with the anticipated molecular size, suggesting the presence of the target oligonucleotides. In the AFM image, ssDNA appears predominantly as dispersed, flexible filamentous strands distributed across the substrate surface (Fig. 3b). The irregular contour of the strands reflects the absence of a stable double-helical architecture, consistent with the intrinsic conformational flexibility of ssDNA. Localized regions of aggregation are occasionally observed, may arise from intermolecular interactions or surface-mediated adsorption[30]. This heterogeneous morphology differs from with the more ordered arrangement expected for dsDNA and may influence dye–DNA interactions and molecular packing density. Such structural differences may affect the local electronic environment of the bound R6G molecules, thereby affecting the extent of Raman signal enhancement.

Raman signal enhancement of R6G on ssDNA

To further study the effect of DNA conformation on Raman enhancement of R6G, the above study on dsDNA was extended to ssDNA where R6G was mixed with ssDNA for Raman signal acquisition, which is schematically represented in (Fig. 3c). Firstly, 1 x 10^{-3} M of R6G was mixed with ssDNA at 50 µg ml^{-1} and Raman signals were acquired. As expected, the Raman signal of R6G on ssDNA was enhanced by an order of magnitude as compared to that in absence of DNA (Fig. 3d). Further, over a concentration range from 5× 10^{-4} M to 1 × 10^{-5} M of R6G the Raman intensity progressively decreased with the concentration. Distinct Raman peaks, however, were detectable down to 2.5 × 10^{-5} M in the presence of ssDNA (Fig. 3e). Notably, a maximum enhancement factor of 50 was achieved, which is more than twice that observed with dsDNA under comparable conditions.

From the Raman signal measurements of R6G on both ds DNA and ss DNA, it is quite evident that nearly an order of magnitude signal enhancement can be achieved on DNA as a substrate. However, the Raman signal does not scale predictably with concentration, evidenced by the absence of a consistent intensity trend in the prominent 1508 cm^{-1} peak (Supplementary Fig. 2), probably due to heterogeneous spatial distribution of the R6G molecules bound dsDNA or ssDNA .A more structurally ordered platform may

mitigate these local variations by providing spatially defined binding sites and a homogeneous molecular environment, thereby improving signal reproducibility and overall, Raman performance. In this context, a rectangular DNA origami nanostructure was investigated as a programmable substrate. Owing to its precisely controlled 2D architecture and high structural rigidity, the origami nanostructure may enable controlled spatial organization of R6G molecules, minimizing its random aggregation and uneven surface distribution. This ordered arrangement is expected to generate a more uniform analyte microenvironment, promote consistent dye–DNA interactions, and might facilitate improved correlation between analyte concentration and Raman intensity.

Design, synthesis and characterization of the rectangular DNA origami nanostructure.

A rectangular DNA origami nanostructure with dimensions 70 × 100 nm was designed with sequence of M13mp18 circular ss DNA as input scaffold in caDNAno [31,32]. The rectangular programmed assembly was achieved by routing the scaffold (Fig. 4a) in 2D architecture consisting of 36 parallel DNA helices and each helix being 190 nucleotides long corresponding to the width and length of the origami design, respectively. The staple sequences obtained as output of designing (Supplementary Table 1) were synthesized commercially. The designed rectangular DNA origami assembly was visualized using UCFchimera[33] for confirming the dimension and structural integrity of the design (Fig. 4b). The designed structure was further evaluated for structural stability, solution-phase conformation, and mechanical flexibility using CanDo[34]. The flexibility map generated from the CanDo simulation, which accounts for thermally induced fluctuations at room temperature, revealed low root-mean-square fluctuations (RMSF) across the majority of the structure, indicative of high global rigidity. Slightly elevated RMSF values were observed at the edges and corners, consistent with the reduced crossover density and boundary effects typically reported for DNA origami nanostructures (Fig. 4c).

The rectangular DNA origami was synthesized through thermal annealing of the scaffold with complementary staple strands, followed by purification using ethanol precipitation (Supplementary Fig. 3). Successful formation of the nanostructure was confirmed by agarose gel electrophoresis. The synthesized DNA origami nanostructure was run against unfolded scaffold and a distinct band appeared with slower migration as compared to the scaffold strand, indicating successful folding of scaffold into a higher molecular weight origami assembly (Fig. 5a). Further characterization by AFM revealed well-defined rectangular nanostructures with dimensions of 70 × 100 (± 5) nm (Fig. 5b) that are in close agreement with the predicted design parameters. Almost all the structures in image exhibited uniform morphology, sharp edges, and minimal structural distortion, indicating high folding efficiency and structural integrity. The narrow size distribution further supports the reproducibility of the assembly process. The line profile across different origami structure show height of the structures to be ~ 2 nm that is in agreement to width of a double helix suggesting a single DNA layer (Fig. 5c). Collectively, these observations confirm the successful formation of the programmed rectangular DNA origami nanostructure and validate its suitability as a structurally ordered platform for subsequent Raman investigations.

Raman signal enhancement of R6G on rectangular DNA origami nanostructures

Drawing inspiration from the Raman signal enhancement observed for the two DNA forms—dsDNA and ssDNA—the study was further extended to rectangular DNA origami nanostructures. R6G was mixed with rectangular DNA origami nanostructures and the Raman signal of bound R6G was acquired, which is schematically illustrated in Fig. 5d. Raman measurements of 1×10^{-3} M R6G in the presence of DNA origami nanostructures at a concentration of 50 μg ml^{-1} demonstrate around two orders of magnitude increase in Raman intensity of R6G as compared to that without DNA (Fig. 5e). On progressively decreasing the R6G concentration from 5×10^{-4} M to 1×10^{-5} M, a corresponding reduction in Raman intensity was observed (Fig. 5f), consistent with the trend noted for other DNA-based substrates examined in this study. Importantly, the intensity of the prominent 1508 cm^{-1} band displayed a clearer concentration-dependent trend, underscoring improved signal consistency and enhanced potential for quantitative analysis unlike that for dsDNA and ssDNA (Supplementary Fig. 2). The lowest detection limit on DNA origami was also improved and R6G could be detected down to 1×10^{-5} M (Fig. 5f) as compared to 2.5×10^{-5} M on the other DNA substrates studied here. Notably, a maximum enhancement of around two orders was achieved which is much better than observed on either dsDNA or ssDNA. Collectively, these results position rectangular DNA origami as a structurally defined 2D biological nanomaterial with controlled planar architecture, resonating with the expanding pursuit of engineered 2D platforms for plasmon-free Raman enhancement strategies.

Building upon this premise, we next investigated whether the concentration of the DNA origami nanostructure influences Raman performance. Specifically, Raman signal enhancement of 5×10^{-5} M R6G was measured on half (25 μg ml^{-1}) and double (100 μg ml^{-1}) the concentration of DNA origami studied earlier (50 μg ml^{-1}). This analysis enables assessment of scaffold density–dependent effects on signal amplification and optimization of substrate loading conditions. As in (Supplementary Fig. 4), it was observed that DNA origami at 50 μg ml^{-1} concentration resulted in the highest signal enhancement, outperforming both lower and higher concentrations. While lower concentration of DNA origami resulted in comparatively weaker signals, likely due to insufficient surface coverage, higher concentration might have led to signal suppression, possibly due to excessive molecular crowding or overlapping of origami structures that hinder effective dye–DNA interactions. These results highlight that an optimal origami concentration is critical for achieving maximum enhancement, by striking the most favorable balance between surface availability and analyte accessibility.

Discussion

This study demonstrates, that DNA can serve as metal-free substrate for enhancing Raman scattering. However, the signal enhancement factor varies across 3 structurally distinct DNA forms: dsDNA, ssDNA, and rectangular DNA origami nanostructure, studied here. A comparative analysis (Fig. 6a) indicates that the DNA origami platform exhibits the highest enhancement of nearly two orders of magnitude followed

by ssDNA and dsDNA. These findings underscore the superiority of the structurally ordered DNA origami nanostructure as a substrate for Raman signal enhancement, relative to either dsDNA or ssDNA substrates.

From the current understanding, Raman signal enhancement on conventional metal-based substrates has been majorly accredited to two phenomenon - electromagnetic enhancement (EE) and CE [35]. The source of EE has been understood to be the plasmon oscillations and thereby local field enhancement around metal nanostructures [36]. CE is believed to be having its origin largely through charge transfer mechanism between closely placed HOMO-LUMO orbitals [37]. In the context of non-metallic substrates, charge transfer has been mostly found to be major contributor for Raman signal enhancement [8,38].

In case of the Raman signal enhancement on DNA as observed in this study, the possible explanations lie in physical accessibility of the dye molecules or/and CE phenomenon on various DNA forms/nanostructure. Looking these aspects in detail, firstly, R6G is known to bind in the minor groove of dsDNA with binding constants ~ 10^6 M^{-1} measured by voltammetry, UV-vis, and fluorescence spectroscopy[39,40]. On the other hand, the binding of R6G to ssDNA is most likely electrostatic, cooperative and non-intercalative, occurring along the flexible ssDNA chain without groove specificity. Single stranded DNA may favor higher affinity via reduced steric hindrance. Though no studies on interaction of R6G with DNA origami have been reported, drawing equals from ds DNA, it can be inferred that the precise geometry and B-form topology of DNA in origami enhances controlled patterned positioning of R6G. Keeping this picture in mind, the origin of Raman signal enhancement may be deciphered as discussed below.

Since R6G binds to DNA, the observed Raman signal enhancement may be attributed to a possible model of CE either a static chemical interaction or through charge transfer. The DNA double helix is known to possess overlapping π–π electron clouds of stacked aromatic nitrogenous bases, which in all probability interact with electron cloud of proximal R6G thereby increasing its polarizability and thus the Raman signal. Evidence of such an interaction was presented in a study where the fluorescence quantum yield of R6G was significantly reduced upon interaction with ds DNA caused by proton-coupled electron transfer between the dye and the guanine bases of the DNA. Here, R6G has been shown to act as the electron acceptor and DNA as the donor[41–43]. Such interaction between R6G and DNA may result in the electron cloud distortion and thereby increasing the polarizability of the R6G molecule and thus, explain the observed enhancement in the Raman signal of the dye.

Further, the differences in the enhancement factors observed on various forms of DNA as substrates, in our study, may be understood through the charge transfer excitation energy of the system which may be determined by the relative alignment of frontier orbitals of the nucleobases and the dye. In native dsDNA, the π-stacked base pairs create delocalized electronic states where G typically possesses the highest HOMO (lowest oxidation potential)[44] while C and T contribute lower-lying orbitals; photoexcitation can therefore promote intrabase or interbase π–π* (HOMO→LUMO) transitions and, under suitable energetic alignment, enable photoinduced electron or hole transfer between bases that subsequently result in the

charge transfer with the dye molecule in proximity [45]. In absence of any direct scientific study that actually demonstrate the HOMO - LUMO energy of R6G upon binding to DNA, we consider reported values for unbound R6G, -5.7 ev and – 3.4 ev for HOMO and LUMO respectively [21,46]. The reported HOMO energy for dsDNA is ~ -5.6 ev [16,47]. In case of ssDNA the increased conformational flexibility and reduced π-stacking alter orbital overlap with HOMO at ~ -5.8 eV [48]. Though the electronic properties of DNA origami are not yet fully understood, simulations have shown that the energies of the occupied orbitals shift to higher energies ~ 4.7 ev as compared to ds DNA[47] (Fig. 6b). These energy values indicate the increased probability of charge transfer to LUMO of R6G when on DNA origami substrate as compared to either ssDNA or dsDNA, resulting in significant Raman signal enhancement. The closely aligned HOMO of both R6G and DNA, potentially enabling resonance-type interactions can further support efficient charge-transfer pathways. As, in DNA origami, the dense and programmable arrangement of helices enhances interhelical coupling and can create extended pathways for exciton migration or hole transfer across stacked domains and from oxidized DNA (e.g., $G^{\bullet+}$) to the dye HOMO which seems energetically favorable[49] .Thus, the observed Raman signal enhancement may be influenced by a combination of factors including orbital energy alignment, stacking geometry, microenvironment, and the structural organization of the DNA substrate.

In conclusion, DNA beyond its traditional role as a genetic carrier, can function as an active molecular scaffold capable of enhancing Raman signals probably through charge-transfer mechanisms. Among the different structural forms studied, DNA origami stood out as an effective Raman signal enhancement substrate, because of its well-organized structure. Moreover, due to its inherent biocompatibility, DNA holds strong potential for in vivo sensing applications, without relying on conventional plasmonic materials. Further, different molecules, especially DNA binding molecules are required to be explored, for signal enhancement on these substrates, to delve into the exact mechanism and potential biosensing applications. Theoretical insights would complement these experimental observations and help establish a more rigorous framework for predicting and optimizing non-plasmonic, chemically enhanced Raman systems based on DNA nanostructures. This will open exciting possibilities for designing multiplexed sensors for clinical diagnosis.

Methods

Plasmid DNA isolation

Double stranded plasmid DNA (pcDNA3.1, Addgene) was isolated using the alkaline lysis method from *Escherichia coli* (DH5α) host cells using a plasmid DNA Midiprep purification kit (HiMedia), following the protocol provided by the manufacturer. The purified plasmid (dsDNA) was subsequently used for downstream characterization and Raman measurements.

Designing and synthesis of DNA origami substrate

The rectangular DNA origami nanostructure was initially designed using caDNAno software, targeting an overall dimension of approximately 70 nm × 100 nm. A square lattice architecture was selected to ensure uniform helix packing and structural rigidity. The design consisted of parallel double-helical domains arranged in a raster pattern, with each helix comprising approximately 190 nucleotides in length. Crossovers between adjacent helices were strategically introduced at intervals corresponding to 1.5 helical turns (~ 16 base pairs), allowing proper alignment of neighboring helices and bringing adjacent minor grooves into close proximity. This crossover positioning minimized torsional strain and enhanced mechanical stability while preserving the intended rectangular geometry. Careful consideration was given to crossover density, staple strand routing, and scaffold path continuity to prevent structural distortion and ensure efficient folding. Coarse-grained simulations were performed using the CanDo platform to evaluate predicted mechanical stability, flexibility, and strain distribution. The structure was subsequently visualized in three dimensions using UCSF Chimera to confirm geometric fidelity prior to experimental fabrication. Based on the optimized design, the generated staple sequences (Supplementary Table 1) were extracted for downstream synthesis of DNA origami.

For assembly, the scaffold (7429 base circular single-stranded M13mp18 DNA; Takara Bio, USA) was used at a final concentration of 1x 10^{-8} M and commercially synthesized short oligonucleotide staple strands (BioServe -a division of ReproCELL, India) were added in a 1:5 scaffold-to-staple molar ratio in 1× Tris-Acetate-EDTA (TAE) buffer, promoting complete hybridization. Magnesium ions were included at a final concentration of 12.5 mM to provide electrostatic screening of the negatively charged phosphate backbone and facilitate proper folding. Thermal annealing was performed in a gradient thermocycler (Recombinant DNA Biosciences Pvt. Ltd, India) by initially heating the mixture to 95°C for 10 minutes to ensure complete denaturation of secondary structures, followed by gradual cooling to 15°C. The cooling ramp was programmed at a rate of 1°C per minute, with the final temperature of 15°C maintained for 10 minutes to stabilize the fully folded origami structures. The synthesized folded nanostructures were purified and concentrated by ethanol precipitation to enhance DNA recovery and maintain folding integrity[50]. The resulting purified DNA origami nanostructure were resuspended in 1x TAE/Mg^{2+} buffer and used for downstream characterization and Raman experiments.

Agarose gel electrophoresis

Agarose gel electrophoresis was performed to validate and assess the structural integrity and purity of the three DNA substrates- DNA origami, plasmid DNA (ds DNA), and single-stranded DNA (ssDNA). All DNA samples were run individually along a 100-10000 bp DNA ladder in a 1% agarose gel cast in 1x TAE buffer, with ethidium bromide incorporated for in-gel nucleic acid staining. Electrophoresis was conducted at 100mV for 1 hour, and the resulting DNA bands were visualized using a gel documentation system.

Atomic Force Microscopy (AFM)

Atomic force microscopy (AFM) was performed for visualization and topographical characterization of DNA (including dsDNA, ssDNA and DNA origami nanostructures) deposited on surface. Samples were

prepared by depositing dilute DNA solutions onto freshly stripped mica substrates and incubating for ~ 5 minutes to promote surface adsorption. Following incubation, the mica surfaces were gently washed with type-I water and then air-dried prior to imaging [51]. Surface topography of the dried DNA was examined using a multimode scanning probe microscope (NT-MDT, SOLVER-PRO). The AFM measurements were performed in tapping mode under ambient conditions, utilizing silicon cantilever tips with a radius of curvature of ~ 10 nm, a spring constant of 5.5 N/m, and a resonance frequency of approximately 115 kHz. Imaging was conducted at multiple locations across several independently prepared samples to ensure consistency and reproducibility.

Raman signal measurement

Raman measurements of R6G were conducted with and without different forms of DNA. The samples were prepared by mixing different concentrations of R6G ranging from 1×10^{-3} M to 1×10^{-5} M with either form of DNA (50 μg ml^{-1}) in 1x TAE/Mg^{2+} buffer and drop casted onto glass coverslips that were thoroughly cleaned earlier by sequential rinsing with acetone, isopropanol, and type-I water.

Raman spectra were acquired using a micro-Raman setup configured in reflection geometry. A 785 nm laser delivering ~ 20mW power at sample plane was focused from bottom using a high NA (60×) oil immersion objective (Olympus) on an inverted microscope (Olympus IX73), producing ~ 1μm spot size. Raman scattering signal was collected using the same objective and the scattered light was directed to a high-resolution spectrograph (Andor, Shamrock 303i, 600 lines/mm grating) coupled to a thermoelectrically cooled CCD detector (− 80°C). Each spectrum was integrated for 10 s. To ensure statistical reliability, five spectra were collected from each drop across three independent experimental sets for each condition. Schematic of Raman setup is shown in (Supplementary Fig. 1.).

Processing of Raman Spectra

The raw Raman signal obtained during the experiments were processed using an iterative polynomial background subtraction method. In brief, the Raman signal was first corrected by subtracting a background signal recorded with the spectrograph in the absence of the analyte under consideration. This Raman signal was then baseline corrected using an iterative polynomial estimation of the background in the signal. Finally, the baseline corrected spectrum were smoothed and averaged over ~ 10 spectral acquisitions to get the final mean Raman spectra and associated standard deviation of the data.

Calculation of Raman Enhancement Factor (EF)

The enhancement factor (EF) was calculated from the obtained Raman spectra using the ratio of Raman intensities normalized by the respective analyte concentrations in the presence of DNA and absence of DNA using the following equation:

$$EF = \frac{I_E \times C_N}{I_N \times C_E}$$

1

where I_E represents the Raman intensity of the 1508 cm^{-1} vibrational mode of R6G, measured in the presence of the respective DNA substrates (ssDNA, dsDNA, or DNA origami). I_N represents the Raman intensity of the same 1508 cm^{-1} vibrational mode of R6G measured in the absence of DNA. C_E corresponds to the concentration of R6G in the presence of DNA, and C_N represents the concentration of R6G measured without DNA[8].

Declarations

Competing interests

The authors declare no competing interest.

Author contributions

P.D. and R.S. conceived the project and designed the study. P.D. and K.G. carried out the DNA origami design. P.D. and N.M were involved in sample preparation. P.D., S.V., A.C and R.S. performed Raman measurements and analyzed the data. C.M. contributed in AFM characterization. P.D., A.C., and R.S. interpreted the results and prepared the original draft of the manuscript. S.K.M supervised the research and reviewed the manuscript. All authors contributed to discussion of the results and approved the final manuscript.

Acknowledgements

The authors acknowledge financial support from the Raja Ramanna Centre for Advanced Technology under the Department of Atomic Energy, India. P.D. acknowledges Homi Bhabha National Institute, India, for a research fellowship.

Data availability:

The data supporting the findings of this study are available from the corresponding author upon reasonable request.

References

1. Long, D. A. *The Raman Effect*. (John Wiley & Sons, Chichester, 2002).
2. Xue, T. *et al.* R6G molecule induced modulation of the optical properties of reduced graphene oxide nanosheets for ultrasensitive SPR sensing. *Scientific Reports* **6**, 1–8 (2016).

3. Lombardi, J. R. & Birke, R. L. A unified view of surface-enhanced Raman scattering. *Accounts of Chemical Research* **42**, 734–742 (2009).
4. Mai, Q. D. *et al.* Silver nanoparticles-based SERS platform towards detecting chloramphenicol and amoxicillin: an experimental insight into the role of HOMO–LUMO energy levels in the SERS signal and charge transfer process. *Journal of Physical Chemistry C* **126**, 7778–7790 (2022).
5. Demirel, G. *et al.* Surface-enhanced Raman spectroscopy: an adventure from plasmonic metals to organic semiconductors as SERS platforms. *Journal of Materials Chemistry C* **6**, 5314–5335 (2018).
6. Zou, S. & Schatz, G. C. Silver nanoparticle array structures that produce giant electromagnetic field enhancements. *Chemical Physics Letters* **403**, 62–67 (2005).
7. Tan, X., Melkersson, J., Wu, S., Wang, L. & Zhang, J. Noble-metal-free materials for surface-enhanced Raman spectroscopy detection. *ChemPhysChem* **17**, 2630–2639 (2016).
8. Majumdar, D. 2D material-based surface-enhanced Raman spectroscopy platforms (either alone or in nanocomposite form): from a chemical enhancement perspective. *ACS Omega* **9**, 40242–40258 (2024).
9. Bhakat, A. & Chattopadhyay, A. Molecular cooperativity in intense Raman scattering on organic molecular microcrystals. *Advanced Optical Materials* **12**, 2301776 (2024).
10. Fularz, A., Almohammed, S. & Rice, J. H. SERS enhancement of porphyrin-type molecules on metal-free cellulose-based substrates. *ACS Sustainable Chemistry & Engineering* **9**, 16808–16819 (2021).
11. Ling, X. *et al.* Raman enhancement effect on two-dimensional layered materials: graphene, h-BN and MoS_2. *Nano Letters* **14**, 3033–3040 (2014).
12. Zadegan, R. M. & Norton, M. L. Structural DNA nanotechnology: from design to applications. *International Journal of Molecular Sciences* **13**, 7149–7162 (2012).
13. Seeman, N. C. Nanomaterials based on DNA. *Annual Review of Biochemistry* **79**, 65–87 (2010).
14. Porath, D., Bezryadin, A., de Vries, S. & Dekker, C. Direct measurement of electrical transport through DNA molecules. *Nature* **403**, 635–638 (2000).
15. Endres, R. G., Cox, D. L. & Singh, R. R. P. Colloquium: the quest for high-conductance DNA. *Reviews of Modern Physics* **76**, 195–214 (2004).
16. Steckl, A. J. DNA: a new material for photonics? *Nature Photonics* **1**, 3–5 (2007).
17. Giese, B. Long-distance charge transport in DNA: the hopping mechanism. *Accounts of Chemical Research* **33**, 631–636 (2000).
18. Wagenknecht, H. A. Electron transfer processes in DNA: mechanisms, biological relevance and applications. *Natural Product Reports* **23**, 973–1006 (2006).
19. Genereux, J. C. & Barton, J. K. Mechanisms for DNA charge transport. *Chemical Reviews* **110**, 1642–1662 (2009).
20. Ferapontova, E. E. Electron Transfer in DNA at Electrified Interfaces. *Chemistry - An Asian Journal* **14**, 3773–3781 (2019).

21. Shao, M.-W. *et al.* An ultrasensitive method: surface-enhanced Raman scattering of Ag nanoparticles from β-silver vanadate and copper. *Chemical Communications* **2008**, 2310–2312 (2008).
22. Liu, D. *et al.* Raman enhancement on ultra-clean graphene quantum dots produced by quasi-equilibrium plasma-enhanced chemical vapor deposition. *Nature Communications* **9**, 193 (2018).
23. Jing, H. *et al.* Impact of adsorbed molecules on the relative intensity of surface-enhanced Raman scattering. *Physical Review B* **111**, 075430 (2025).
24. Yilmaz, M. *et al.* Nanostructured organic semiconductor films for molecular detection with surface-enhanced Raman spectroscopy. *Nature Materials* **16**, 918–924 (2017).
25. Song, X. *et al.* Two-orders-of-magnitude enhancement of SERS activity via simple surface engineering of quasi-metal single-crystal frameworks. *Nano Letters* **24**, 11683–11689 (2024).
26. Kamens, J. The Addgene repository: an international nonprofit plasmid and data resource. *Nucleic Acids Research* **43**, D1152–D1157 (2015).
27. Tanigawa, M. & Okada, T. Atomic force microscopy of supercoiled DNA structure on mica. *Anal. Chim. Acta* **365**, 19–25 (1998).
28. Lyubchenko, Y. L. & Shlyakhtenko, L. S. Visualization of supercoiled DNA with atomic force microscopy in situ. *Proc. Natl. Acad. Sci. U. S. A.* **94**, 496–501 (1997).
29. Luo, L. B. Surface-enhanced Raman scattering from uniform gold and silver nanoparticle-coated substrates. *Journal of Physical Chemistry C* **113**, 9191 (2009).
30. Sharipov, T. *et al.* Scanning tunneling spectroscopy of homooligonucleotides. *Eurasian Journal of Physics and Functional Materials* **7**, 232–238 (2023).
31. Douglas, S. M. *et al.* Rapid prototyping of 3D DNA-origami shapes with caDNAno. *Nucleic Acids Research* **37**, 5001–5006 (2009).
32. Castro, C. E. *et al.* A primer to scaffolded DNA origami. *Nature Methods* **8**, 221–229 (2011).
33. Pettersen, E. F. *et al.* UCSF Chimera: a visualization system for exploratory research and analysis. *Journal of Computational Chemistry* **25**, 1605–1612 (2004).
34. Kim, D. N., Kilchherr, F., Dietz, H. & Bathe, M. Quantitative prediction of 3D solution shape and flexibility of nucleic acid nanostructures. *Nucleic Acids Research* **40**, 2862–2868 (2012).
35. Schlücker, S. Surface-enhanced Raman spectroscopy: concepts and chemical applications. *Angewandte Chemie International Edition* **53**, 4756–4795 (2014).
36. Han, X. X. *et al.* Surface-enhanced Raman spectroscopy. *Nature Reviews Methods Primers* **1**, 87 (2022).
37. Chen, R. & Jensen, L. Interpreting chemical enhancements of surface-enhanced Raman scattering. *Chemical Physics Reviews* **4**, 021305 (2023).
38. Hao, Q. *et al.* Surface-enhanced Raman scattering study on graphene-coated metallic nanostructures. *Journal of Physical Chemistry C* **116**, 7249–7254 (2012).
39. Al Masum, A. *et al.* Biochemical activity of rhodamine 6G: molecular modeling and spectroscopic studies. *Journal of Photochemistry and Photobiology B* **164**, 369–379 (2016).

40. Letuta, S. N. *et al.* Interaction of rhodamine 6G with DNA studied by spectrophotometry. *Optics and Spectroscopy* **93**, 844–847 (2002).
41. Neubauer, H. *et al.* Dynamics of rhodamine 6G attached to DNA revealed by spectroscopy. *Journal of the American Chemical Society* **129**, 12746–12755 (2007).
42. Seidel, C. A. M., Schulz, A. & Sauer, M. H. M. Nucleobase-specific quenching of fluorescent dyes. *Journal of Physical Chemistry* **100**, 5541–5553 (1996).
43. Lietard, J., Ameur, D. & Somoza, M. M. Sequence-dependent quenching of fluorescein fluorescence on DNA. *RSC Advances* **12**, 5629 (2022).
44. Xiang, L. *et al.* Gate-controlled conductance switching in DNA. *Nature Communications* **8**, 14471 (2017).
45. Nguyen, T. X. *et al.* Kinetics of Photoinduced Electron Transfer between DNA Bases and Triplet 3,3',4,4'-Benzophenone Tetracarboxylic Acid in Aqueous Solution of Different pH's: Proton-Coupled Electron Transfer? *J. Phys. Chem. A* **116**, 10668 (2012).
46. Bhatia, H., Dhakate, S. R. & Subhedar, K. M. Enhanced SERS signal in graphene-based hybrid substrates. *Diamond and Related Materials* **150**, 111734 (2024).
47. Demir, B. *et al.* Electronic properties of DNA origami nanostructures revealed by simulations. *Journal of Physical Chemistry B* **128**, 4646–4654 (2024).
48. Murti, B. T. *et al.* Light-induced DNA-functionalized TiO_2 interfaces for sensing. *Journal of Photochemistry and Photobiology B* **188**, 159–176 (2018).
49. Shang, E. *et al.* Inter-helical excitonic coupling dye assemblies templated with anti-parallel and parallel DNA motifs. *Nanoscale* **17**, 25281–25288 (2025).
50. Lei, Y. *et al.* Purification and concentration of DNA origami structures by ethanol precipitation. *ChemNanoMat* **8**, 5917-5923 (2022).
51. Pillers, M. A. *et al.* Preparation of mica and silicon substrates for DNA origami analysis. *Journal of Visualized Experiments* **2015**, 1–8 (2015).
52. Mehmandoust, S., Eskandari, V. & Karooby, E. Fabrication of DNA origami plasmonic structures for SERS platforms. *Plasmonics* **19**, 1131–1143 (2024).

Figures



Figure 1

Schematic depicting mix of R6G and DNA drop-casted onto glass coverslip for Raman signal measurements. In this study varying concentrations of R6G are mixed with fixed concentrations of different forms of DNA, either ds DNA, ss DNA or 2D rectangular DNA origami nanostructures and drop casted onto glass coverslips for subsequent measurement of Raman spectra using 785 nm Laser as excitation source.

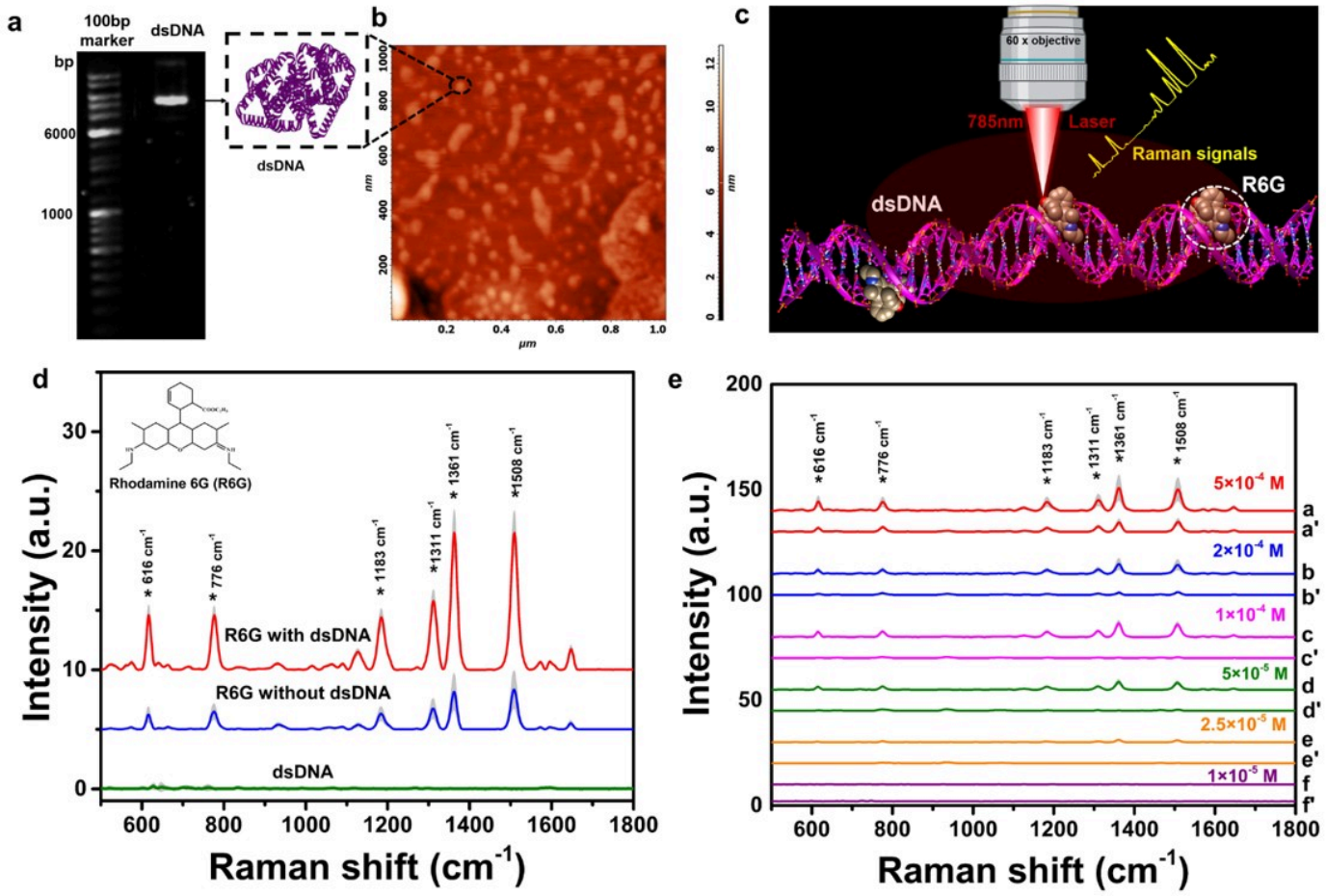


Figure 2

Characterization of the isolated dsDNA and Raman detection of R6G with it. (a) Agarose gel electrophoresis revealed the characteristic twin-band pattern of plasmid DNA, with the faster-migrating supercoiled isoform resolving near 8 kbp DNA ladder marker. (b) AFM image of isolated and purified dsDNA deposited on mica, demonstrating small clusters comprising of multiple molecules in condensed conformation. Inset depicts cartoon representation of ds DNA. (c) A schematic illustration of R6G bound to ds DNA upon mixing, for Raman signal acquisition. (d) Raman spectra of 1×10^{-3} M R6G in presence of dsDNA substrate demonstrate significant enhancement of the Raman intensities as compared to that in absence of dsDNA. The spectrum of ds DNA alone is shown as control. Molecular structure of R6G dye is shown as inset (e). Raman spectra of varying concentrations of R6G (a–f) (5×10^{-4} M- 1×10^{-5} M) on dsDNA and (a'–f') are corresponding Raman spectra of R6G without ds DNA. As evident from the spectra that R6G can be detected down to 2.5 x 10^{-5} M on ds DNA but only up to 1 x 10^{-4} M in absence of ds DNA. All the spectra are vertically offset along the y-axis for clarity of presentation. The error bars are shown as grey background and represent ±1 standard deviation.

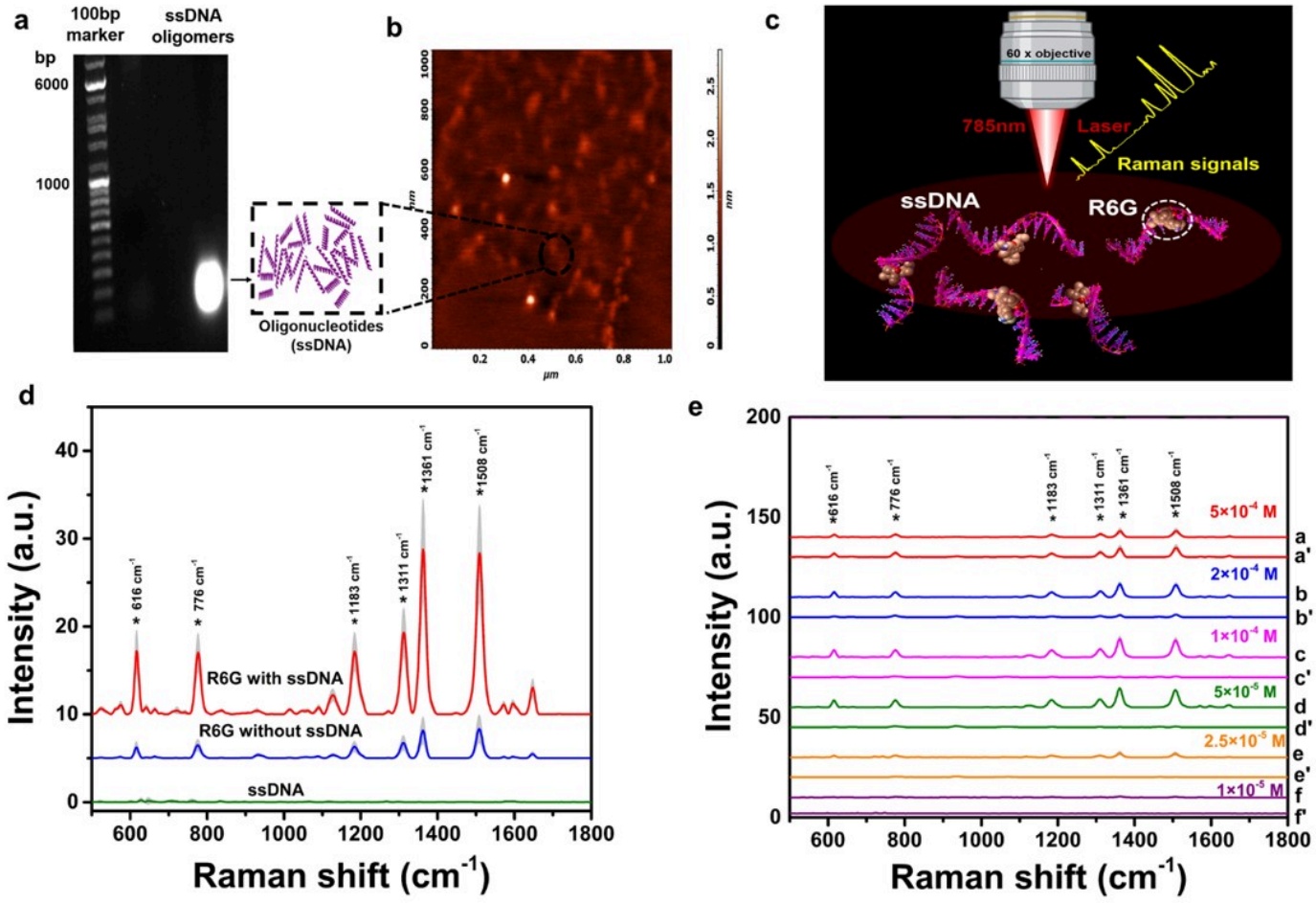


Figure 3

Electrophoretic and microscopic characterization of the ssDNA cocktail and Raman measurements of R6G with it. (a) Agarose gel electrophoresis revealed a diffuse band with long migration suggesting presence of short oligonucleotides with variable sizes. (b) AFM image showing distributed flexible strands of ssDNA with few areas of intermolecular aggregation. Inset depicts cartoon representation of ss DNA. (c) A schematic representation of R6G bound to ss DNA upon mixing prior to Raman signal acquisition. (d) Raman spectra of 1×10^{-3} M R6G in presence of ssDNA demonstrating significant enhancement of the Raman characteristic bands of R6G as compared to that in absence of ssDNA. The spectrum of ssDNA alone is shown as control. (e). Raman spectra of varying concentrations of R6G (a–f) (5×10^{-4} M- 1×10^{-5} M) on ssDNA with (a'–f') being corresponding Raman spectra of R6G without DNA. The spectra show that R6G can be detected down to 2.5 x 10^{-5} M on ssDNA. All the spectra are vertically offset along the y-axis for clarity of presentation. The error bars are shown as grey background and represent ±1 standard deviation.

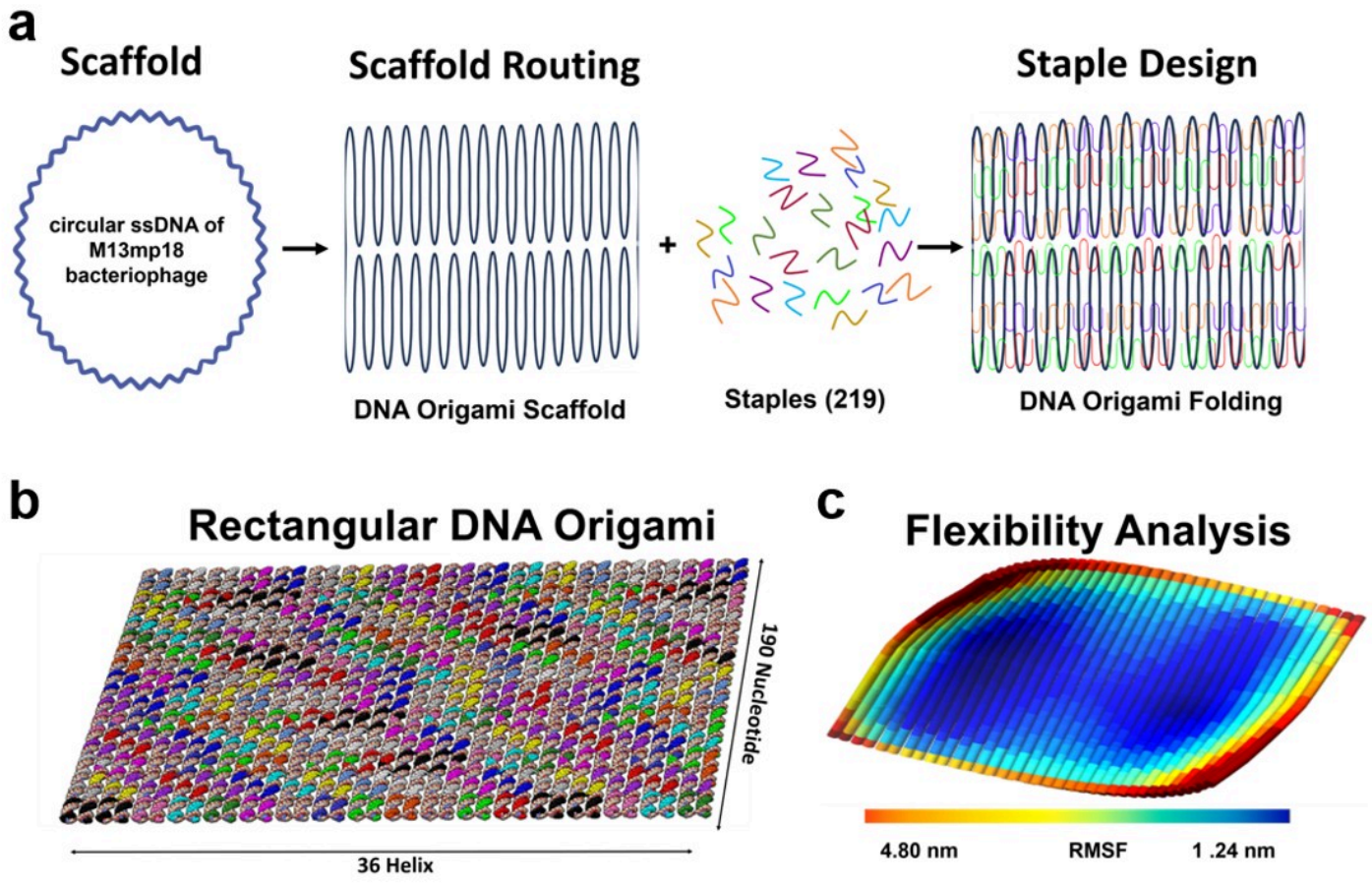


Figure 4

Design of rectangular DNA origami nanostructure (a) Illustration of designing of rectangular DNA origami using caDNAno. The method involves scaffold routing using M13mp18 ss DNA sequence and staple sequence generation for proper rectangular DNA origami folding. (b) Visualization of the output origami structure of the CaDNAno using UCFChimera, confirming shape and dimensions. (c) CanDo predicted flexibility across designed rectangular DNA origami structure demonstrates mostly rigid global structure with highly flexible edges.

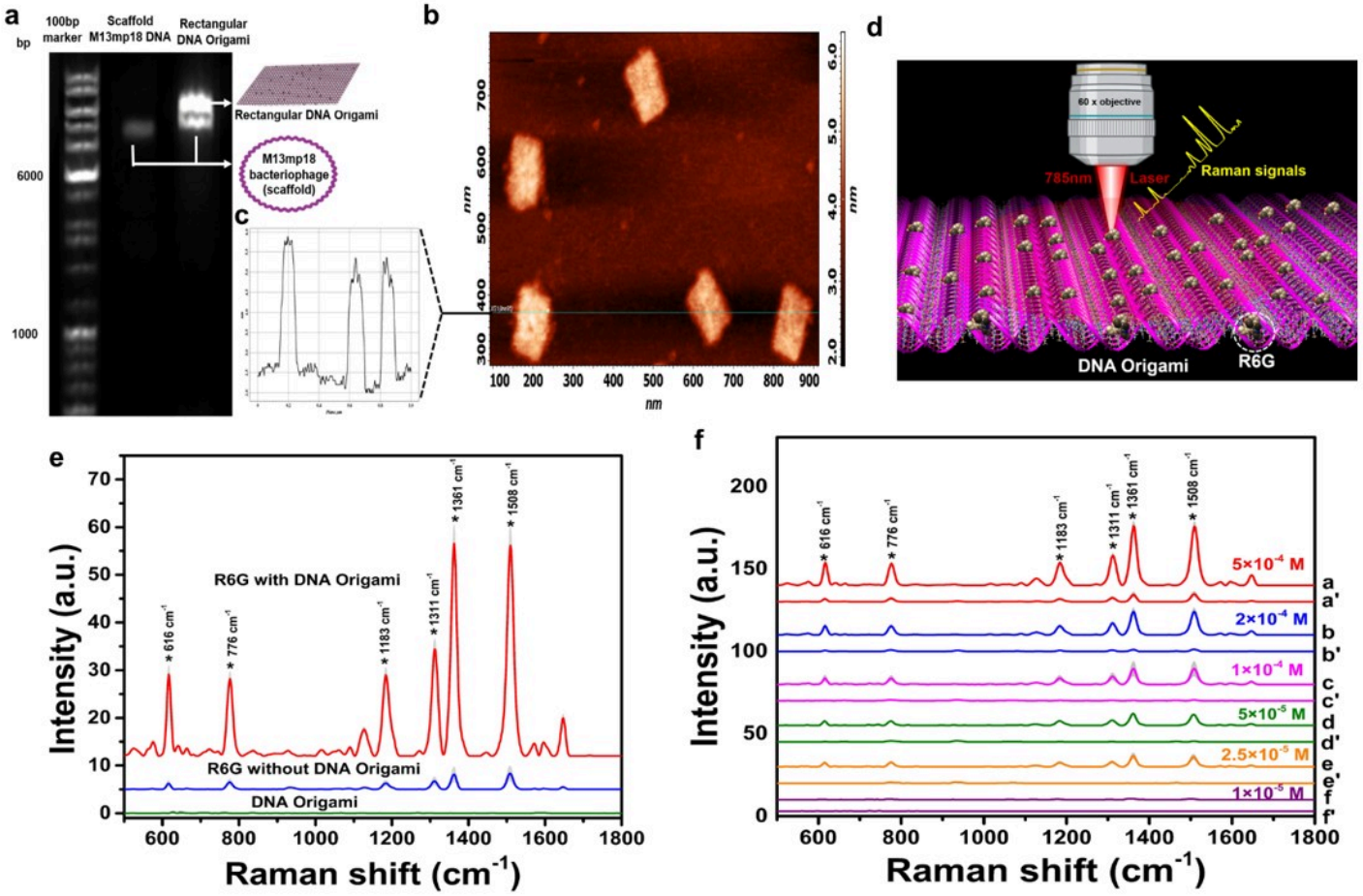


Figure 5

Characterization of the synthesized rectangular DNA origami nanostructure and Raman measurement of R6G on it. (a) Agarose gel electrophoresis revealed a slower-migrating DNA origami band as compared to unfolded scaffold. Inset depicts cartoon representation of DNA origami and M13mp18 DNA corresponding to the band positions on agarose gel. (b) AFM image of purified DNA origami nanostructures demonstrate synthesis of well-defined 2D structure with dimensions of 70 × 100 (±5) nm. (c) The line profile across the DNA origami structures shows a height of ~2 nm, corresponding to a single DNA layer and consistent with the diameter of the DNA double helix. (d) A schematic illustration of R6G bound to DNA origami nanostructure. (e) Raman spectra of 1×10^{-3} M R6G with DNA origami demonstrates significant enhancement of the Raman intensities as compared to that in its absence. The spectrum of DNA origami alone is shown as control. (f). Raman spectra of varying concentrations of R6G (a–f) (5×10^{-4} M- 1×10^{-5} M) on rectangular DNA nanostructure with (a'–f') are corresponding Raman spectra of R6G without DNA. The spectra show that R6G can be detected down to 1.0×10^{-5} M on DNA origami. All the spectra are vertically offset along the y-axis for clarity of presentation. The error bars are shown as grey background and represent ±1 standard deviation.

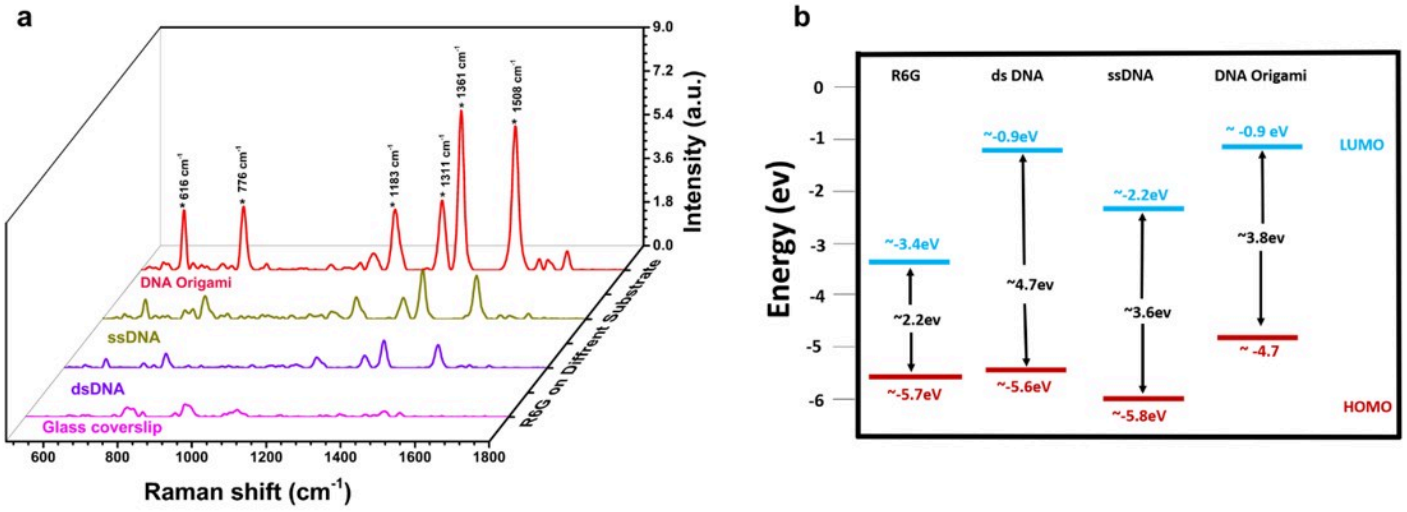


Figure 6

Comparison of Raman signal enhancement of R6G (2.5 × 10^{-5} M) on different DNA substrates—dsDNA, ssDNA, rectangular DNA origami nanostructures—and their reported HOMO–LUMO energy levels, highlighting the relationship between electronic structure and Raman enhancement. (a) In comparison to dsDNA and ssDNA, maximum Raman enhancement for R6G is observed with DNA origami as substrate. (b) The reported HOMO–LUMO energy levels of R6G and the DNA architectures studied here indicate a greater likelihood of charge transfer to the LUMO of R6G when adsorbed on the DNA origami substrate compared to ssDNA or dsDNA, thereby leading to significant Raman signal enhancement.

Supplementary Files

This is a list of supplementary files associated with this preprint. Click to download.

- supplementryinformation20032026Revised.docx